Journal of Biomedical Optics

BiomedicalOptics.SPIEDigitalLibrary.org

Three-dimensional optical coherence elastography by phase-sensitive comparison of C-scans

Brendan F. Kennedy
Francisco Gomes Malheiro
Lixin Chin
David D. Sampson

SPIE.

Three-dimensional optical coherence elastography by phase-sensitive comparison of C-scans

Brendan F. Kennedy,[a,*] Francisco Gomes Malheiro,[a] Lixin Chin,[a] and David D. Sampson[a,b]
[a]The University of Western Australia, School of Electrical, Electronic and Computer Engineering, Optical+Biomedical Engineering Laboratory, 35 Stirling Highway, Crawley, Western Australia 6009, Australia
[b]The University of Western Australia, Centre for Microscopy, Characterisation and Analysis, 35 Stirling Highway, Crawley, Western Australia 6009, Australia

Abstract. We present an acquisition method for optical coherence elastography (OCE) that enables acquisition of three-dimensional elastograms in 5 s, an order of magnitude faster than previously reported. In this method, based on compression elastography, the mechanical load applied to the sample is altered between acquisitions of consecutive optical coherence tomography volume scans (C-scans). The voxel-by-voxel phase difference between the volumes is used to determine the axial displacement and determining the gradient of the axial displacement versus depth gives the local axial strain. We demonstrate sub-100-microstrain sensitivity and high contrast in elastograms, acquired in 5 s, of structured phantoms and freshly excised rat muscle tissue that are comparable in strain sensitivity and dynamic range to our previously reported B-scan-based method. The much higher acquisition speed may expedite the translation of OCE to clinical and *in vivo* applications. [DOI: 10.1117/1.JBO.19.7.076006]

Keywords: optical coherence tomography; optical coherence elastography; strain; biomechanics.

Paper 140284R received May 5, 2014; revised manuscript received Jun. 6, 2014; accepted for publication Jun. 9, 2014; published online Jul. 7, 2014.

1 Introduction

Elastography is an imaging technique that maps variations in tissue stiffness into images, known as elastograms.[1] As tissue stiffness is often closely linked with pathology,[2] elastography has been developed to aid in the diagnosis of disease.[3] Optical coherence tomography (OCT)-based elastography, known as optical coherence elastography (OCE), is an emerging technique that provides higher spatial resolution than more established techniques based on ultrasound and magnetic resonance imaging (MRI).[4,5] Over the last decade, advances in OCT technology, particularly the emergence of spectral-domain OCT, have provided opportunities to make significant improvements in OCE elastogram quality[5] over earlier time-domain OCT systems.[4,6–10] Proposed OCE techniques have been based on a variety of loading methods, including compression,[11–17] surface acoustic wave and shear wave generation,[18–21] internal loading using magnetic nanoparticles,[22,23] and acoustic radiation force.[24–27] The use of OCE is being explored in a range of potential clinical applications, particularly in breast cancer,[16,28,29] dermatology,[30–33] ophthalmology,[20,21,34,35] and cardiology.[6–8,25,36,37]

Recently, several groups have extended OCE to three-dimensional (3-D) imaging.[16,24,25,33] Assessment of tissue volumes is likely to be a key feature in clinical applications of OCE, as is proving to be the case in OCT,[38] and emulates 3-D medical imaging techniques such as MRI[39] and computed tomography (CT).[40] An additional feature, of particular importance in compression OCE, is that 3-D imaging allows elastograms to be visualized in the *en face* plane, with resolution matched to that of the underlying OCT image.[5] Previously reported 3-D-OCE methods have been limited to long acquisition times. In the first demonstration, *in vivo* 3-D elastograms of human skin were acquired in 5 min.[33] More recently, 3-D OCE was demonstrated on excised human coronary artery,[25] with a B-scan acquisition time of 0.1 s, implying a 3-D-OCE scan consisting of 500 B-scans was acquired in 50 s. Such long acquisition times are likely to restrict the application of 3-D OCE in many clinical and *in vivo* applications.

Here, we demonstrate a new acquisition method for compression 3-D OCE, which allows volumes (*xyz*-dimensions, 5 mm × 5 mm × 2 mm) to be acquired in 5 s, at least 10 times faster than that reported using existing 3-D-OCE methods. Although previous methods determine the phase difference between A-scans[41] or B-scans,[12,13,16] our method is based on phase-sensitive detection between volumes (C-scans). A compressive load is imparted between consecutive C-scan acquisitions and the phase difference is calculated between the volumes. We show that the displacement and strain sensitivity of our C-scan method are comparable to the existing B-scan method[5,13,16] and present sub-100-microstrain sensitivity, high-contrast, single-acquisition elastograms generated by compression 3-D OCE of structured phantoms and rat skeletal muscle.

2 Methods

The OCE system is based on an optical fiber-based, spectral-domain OCT system with maximum A-scan rate of 100 kHz and a measured sensitivity of 98 dB for an exposure time of 5 μs used in all measurements reported here. The system employs a superluminescent diode with a central wavelength, λ_0, of 835 nm and a 3-dB bandwidth of 50 nm. The measured axial and lateral resolutions in air (full-width at half-maximum of irradiance) are 8.5 and 11 μm, respectively. The sample arm

*Address all correspondence to: Brendan Kennedy, E-mail: brendan.kennedy@uwa.edu.au

0091-3286/2014/$25.00 © 2014 SPIE

comprises an imaging window fixed to a ring actuator, as described previously,[13,31,42] enabling mechanical loading and imaging from the same side of the sample. An upper brass plate with a surface area of 16 cm^2 was used to apply a preload to ensure that the sample surface was evenly loaded before 3-D-OCE scanning. A square-wave electrical signal was used to drive the ring actuator motion and was synchronized with either the B-scan or C-scan acquisition, as illustrated in Fig. 1. Using this setup, a maximum displacement of 2 μm could be applied to the sample surface. The depth-resolved axial displacement was determined at each lateral position by calculating the phase difference, $\Delta\phi$, at each point between loaded, ϕ_2, and unloaded, ϕ_1, B-scan or C-scan pairs, as shown in Fig. 1, and by performing phase unwrapping to remove the 2π phase ambiguity.[16] The local strain was calculated as the slope of axial displacement, d, over a finite axial range depth using a weighted-least squares fitting algorithm described previously.[13] In the elastograms presented here, the axial fitting range, which we define as the strain axial resolution, is 100 μm, and the strain lateral resolution matches that of the underlying OCT system, i.e., 11 μm.

In the B-scan 3-D-OCE method,[16] oversampling was performed: an OCT B-scan comprising 1000 A-scans was acquired for every 1 μm scanned in the lateral (y-) direction. Although this sampling results in additional phase noise, it is a convenient means of ensuring sufficiently small y-direction offsets between scans to enable effective phase-sensitive detection.[43] The B-scan acquisition (indicated by "x-scanning" in Fig. 1) was synchronized with the mechanical loading [Figs. 1(a) and 1(c)], ensuring that consecutive B-scans were acquired in alternate loading states. To scan a 5 mm × 5 mm × 2 mm volume, 5000 B-scans (2500 unloaded and 2500 loaded) were acquired. The A-scan acquisition time was 100 μs (B-scan acquisition time, 0.1 s) and the loading frequency was 5 Hz, resulting in a total acquisition time of 500 s. In this method, the dependency of B-scan acquisition frequency on mechanical loading frequency [Fig. 1(c)] and the requirement of quasistatic loading, fundamentally limit the 3-D-OCE acquisition speed to this relatively long acquisition time. The condition of quasistatic loading requires that the loading frequency is low enough (<5 Hz) that inertial components in the governing equations of motion can be ignored.[1] Quasistatic loading is a requirement in compression OCE, as it removes the need to consider mechanical wave propagation in the sample, allowing local strain to be used as a contrast mechanism.[1,5]

In the C-scan method, the acquisition was synchronized with the mechanical loading [Figs. 1(b) and 1(d)], ensuring that consecutive C-scans were acquired in alternate loading states [Fig. 1(b)]. As no oversampling was required, the C-scan method required less densely sampled acquisition. Each C-scan comprised 500 B-scans and, in turn, each B-scan comprised 500 A-scans. The OCT acquisition times were 10 μs for an A-scan, 5 ms for a B-scan, and 2.5 s for a C-scan, thus, the total acquisition time for 3-D OCE was 5 s. Because the B-scan acquisition is decoupled from the loading frequency, the acquisition speed is greatly increased, while quasistatic loading is maintained.

To compare the strain sensitivity and elastogram quality of the two methods, two cylindrical tissue-mimicking phantoms with a diameter and thickness of 15 and 2 mm, respectively, were fabricated using silicone elastomers, as described previously.[44,45] Optical scattering in the phantoms was introduced using titanium dioxide particles (refractive index ~2.5, mean diameter ~1 μm). The Young's modulus of the phantoms was controlled by varying the ratio of silicone, the associated curing agent, and non-cross-linked silicone oil and was measured using compression testing.[45] Phantom 1 is optically and mechanically homogeneous and was used to determine the strain sensitivity. The scatterer concentration is 1.5 mg/ml and the Young's modulus is 20 kPa. Phantom 2 was used to compare the elastogram quality of the two methods. This phantom consists of a soft bulk medium (scatterer concentration 1.5 mg/ml, Young's modulus 20 kPa) within which an

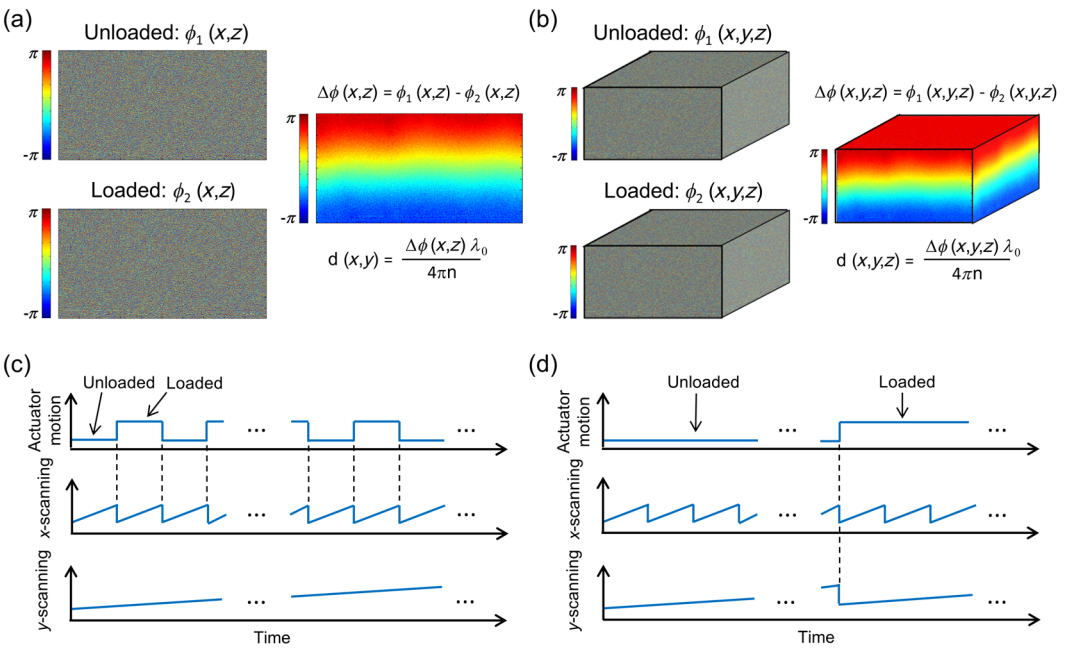

Fig. 1 Schematic diagram illustrating phase-sensitive detection using (a) the B-scan method[16] and (b) the C-scan method; (c) and (d) illustrations of the synchronization between lateral (x- and y-) scanning and mechanical loading for each method.

approximately cuboid stiff inclusion (scatterer concentration 3.5 mg/ml, Young's modulus 837 kPa) is embedded.

3 Results

To compare the performance of each method, we first define the displacement sensitivity as the standard deviation, σ_D, of 50 displacement measurements acquired from the same location on the surface of a stationary layered adhesive tape phantom. The chosen location had a corresponding OCT signal-to-noise ratio (SNR) of ~50 dB. In Fig. 2, histograms of the displacements measured using the B-scan [Fig. 2(a)] and C-scan [Fig. 2(b)] methods are shown. The corresponding displacement sensitivity, calculated as the standard deviation, is 0.63 and 0.86 nm, respectively (as shown in Table 1), corresponding to respective phase sensitivities of 13.3 and 18.1 mrad. The slightly lower displacement and phase sensitivities of the C-scan method are likely due to the small positioning error of the *y*-scanning galvanometer mirror between C-scan acquisitions. In the C-scan method, phase drift in the interferometer caused by environmental conditions may also lower the displacement sensitivity, although this effect is expected to be small for the short acquisition times used here.

Next, the strain sensitivity of both methods was determined using Phantom 1. The phantom was preloaded by translating the upper brass plate ~200 μm from the point of first contact with the phantom (~10% strain). Following preload, a delay of at least 1 min was allowed to ensure the effects of viscoelastic creep had subsided. An additional periodic displacement of 2 μm was then imparted with the ring actuator and the local strain was calculated as described above. We define the strain sensitivity, σ_ε, as the standard deviation of local strain calculated from 50 local strain measurements at adjacent lateral positions in the central region of the phantom.[13] The measured strain sensitivity of the B-scan and C-scan methods, as shown in Table 1, is 85 and 90 $\mu\varepsilon$, respectively. The strain sensitivity was determined from strain measurements over 100 μm, commencing at 20 μm from the phantom surface. The results in Fig. 2 and Table 1 demonstrate that, for the same voxel dwell time, the C-scan method has comparable displacement and strain sensitivity to the B-scan method, but with a 100-fold shorter acquisition time.

In Fig. 3, we present 3-D-OCE results of Phantom 2 acquired with both the B-scan and C-scan methods. Figures 3(a) and 3(b) show the 3-D visualizations, Figs. 3(c) and 3(d) show the depth (*xz*) sections, and Figs. 3(e) and 3(f) show the *en face* (*xy*) images from the depth indicated by the dashed blue lines in Figs. 3(c) and 3(d). Using both methods, high contrast is observed between the stiff inclusion and the soft surrounding material. As expected, the local strain is close to zero in the inclusion, confirming its high stiffness relative to the surrounding soft material. The strain sensitivity was increased in the B-scan method by averaging five loaded/unloaded B-scan pairs, resulting in an increased contrast compared to the C-scan method, while maintaining the lateral resolution of the underlying OCT system (11 μm). B-scan spatial averaging was not performed for the C-scan method, as it would result in elastograms with significantly lower lateral resolution in this more sparsely sampled scan. In Figs. 4 and 5, we demonstrate an equivalent averaging technique for the C-scan method that improves contrast without degrading lateral resolution by averaging multiple C-scan (rather than B-scan) pairs.

Figures 3(a), 3(c), and 3(e) demonstrate a noticeable artifact caused by the limited response time of the actuator when using the B-scan method. Following the step increment in load between B-scans [Fig. 1(c)], a damped oscillation (ringing) of the actuator, indicated by the arrows in Fig. 3, persists for ~25 ms and results in modulation of local strain in the sample. This ringing artifact is confined to the first B-scan in the C-scan method [Figs. 3(b), 3(d) and 3(f)], as the step increment in load is imparted only once with increased rise time between C-scan acquisitions (Fig. 1).

To demonstrate the C-scan method in tissue, *en face* OCT images and elastograms of freshly excised gastrocnemius rat muscle tissue are presented in Fig. 4. In the OCT image [Fig. 4(a)], groups of muscle fibers are visible running from bottom left to top right of the image. Many of these muscle fibers are visible in the elastogram [Fig. 4(b)]. The elastogram also identifies the boundary of several fascicles (bundles of muscle fibers surrounded by a sheath of connective tissue) not readily visible in the OCT image. To better illustrate the complementary contrast provided by OCE, Figs. 4(c) and 4(d) show magnifications of the regions highlighted by the blue rectangle in Figs. 4(a) and 4(b), respectively.

Figure 4(e) demonstrates that improved strain sensitivity can be achieved by trading off sensitivity and acquisition speed. Figure 4(e) shows the results of averaging five loaded and

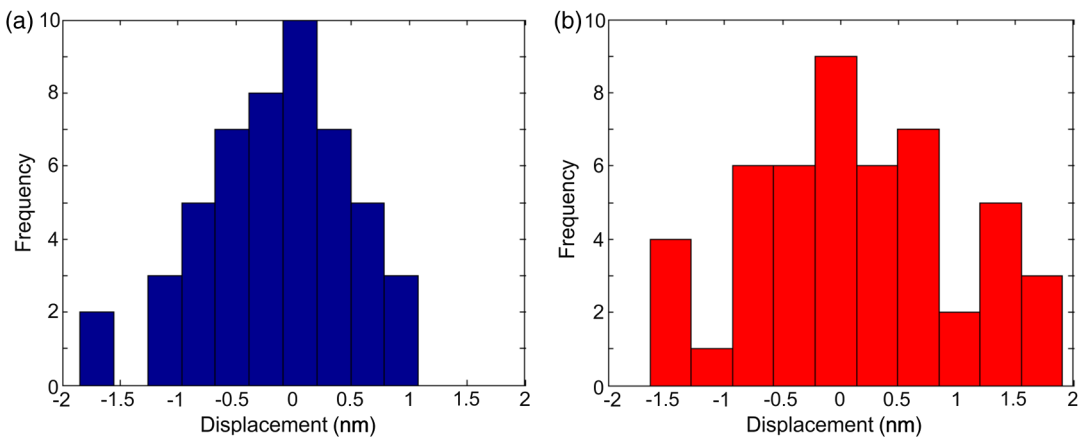

Fig. 2 Histogram of 50 displacement measurements obtained from adjacent lateral locations at the same depth near the surface of a stationary adhesive tape phantom for (a) the B-scan method and (b) the C-scan method.

Table 1 Displacement sensitivity, strain sensitivity, and acquisition time of 3-D-OCE scans using the B-scan and C-scan methods.

Method	σ_D (nm)	σ_ε ($\mu\varepsilon$)	Acquisition time (s)
B-scan	0.63	85	500
C-scan	0.86	90	5

unloaded C-scans acquired from the same spatial location, demonstrating lower noise than in Fig. 4(d). This is analogous to the improved contrast shown in Fig. 3(e) obtained by averaging multiple loaded/unloaded B-scans. Although this increases the total 3-D-OCE acquisition time from 5 to 25 s, an improvement in strain sensitivity is gained. For example, in the bottom right of Fig. 4(e), additional fibers can be seen that are not readily visible in the original elastogram [Fig. 4(d)].

To quantify the improvement in strain sensitivity brought about by averaging in the C-scan method, we acquired 25 loaded and unloaded C-scan pairs from the same location in Phantom 1. Using the method described above, we calculated the strain sensitivity as a function of the number of scans averaged. As shown in Fig. 5, averaging led to an increase in the strain sensitivity from 90 to 60 $\mu\varepsilon$, while the acquisition time increased from 5 to 125 s. Under the assumption of Gaussian-distributed phase, averaging would improve displacement and strain sensitivity by $1/\sqrt{N}$, where N is the number of volumes averaged. The data in Fig. 5 approximately follow this trend. However, while this assumption is valid for shot-noise limited detection,[46] additional phase noise caused by phase decorrelation between loaded and unloaded volumes and scanning noise caused by the galvanometer mirrors lower the phase sensitivity in 3-D-OCE. As a result, the magnitude of the improvement shown in Fig. 5 is less than anticipated.

4 Discussion

We have presented a new method of achieving higher speed acquisition in 3-D-OCE, based on phase-sensitive detection of consecutive C-scans, and demonstrated the acquisition of 3-D-OCE scans in 5 s. The acquisition time was limited by the maximum A-scan rate of the spectral-domain OCT system (100 kHz) and could be readily reduced by using a higher speed OCT system. OCT C-scan acquisition times of only 25 ms have been demonstrated using high-speed swept sources,[47] implying 3-D-OCE scans could be acquired in as little as 50 ms using our method. In practice, the need for quasistatic loading (loading frequency <5 Hz) in compression OCE limits the 3-D-OCE acquisition time to 0.2 s, a further factor of 25 improvement over what has been demonstrated here.

Phase-sensitive detection between volumes overcomes a fundamental limitation of the B-scan method by coupling the loading frequency with the C-scan acquisition frequency. Thus, the need to operate in the quasistatic regime sets the volume scan rate, rather than the B-scan frame rate, to 5 Hz.

The strain sensitivity we report for both B-scan and C-scan methods, 60 to 90 $\mu\varepsilon$, is lower than that previously reported for two-dimensional compression OCE (~2 to 26 $\mu\varepsilon$).[12,16,42] As our group has previously described in detail,[13] a key factor limiting strain sensitivity is OCT SNR, as it determines the achievable

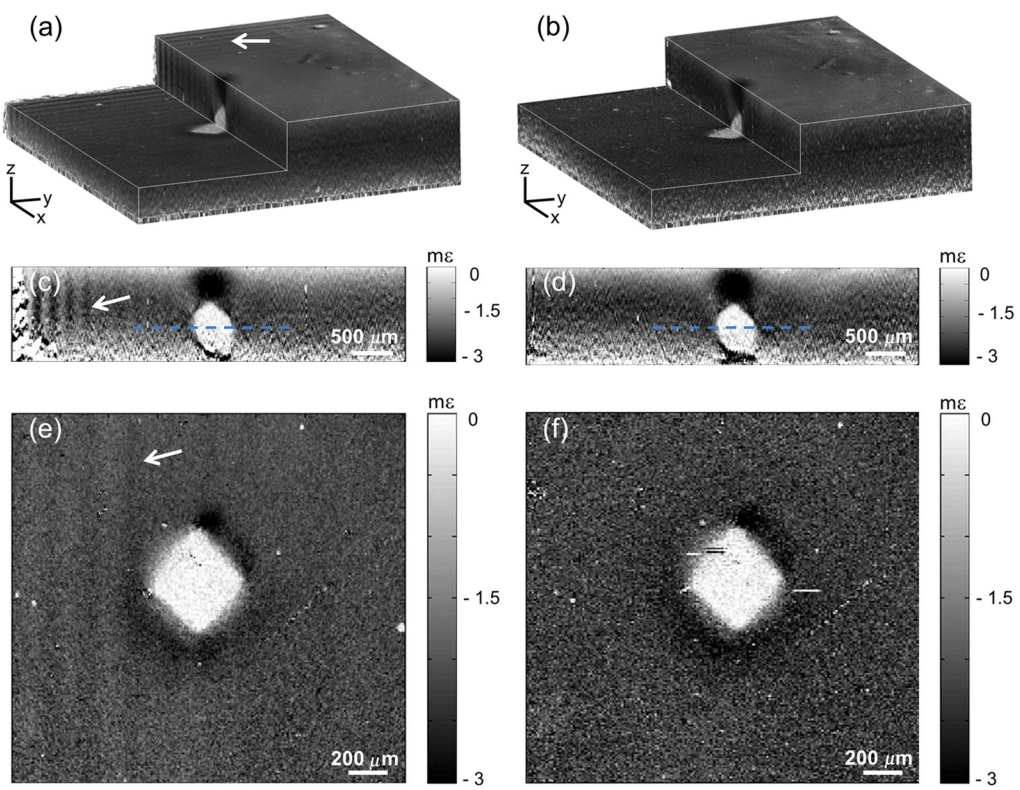

Fig. 3 3-D-OCE elastograms of Phantom 2 acquired with: (a, c, and e) the B-scan method in 500 s; and (c, d, and f) the C-scan method in 5 s. (a and b) 3-D visualizations demonstrating both methods; (c and d) B-scan images (*xz*-plane) from the center of the 3-D volumes in (a) and (b), respectively; (e and f) corresponding *en face* images (*xy*-plane) at the location indicated by the dashed blue line in (c) and (d). The white arrows indicate the ringing artifact. In (a) and (b), scale bars represent 200 μm.

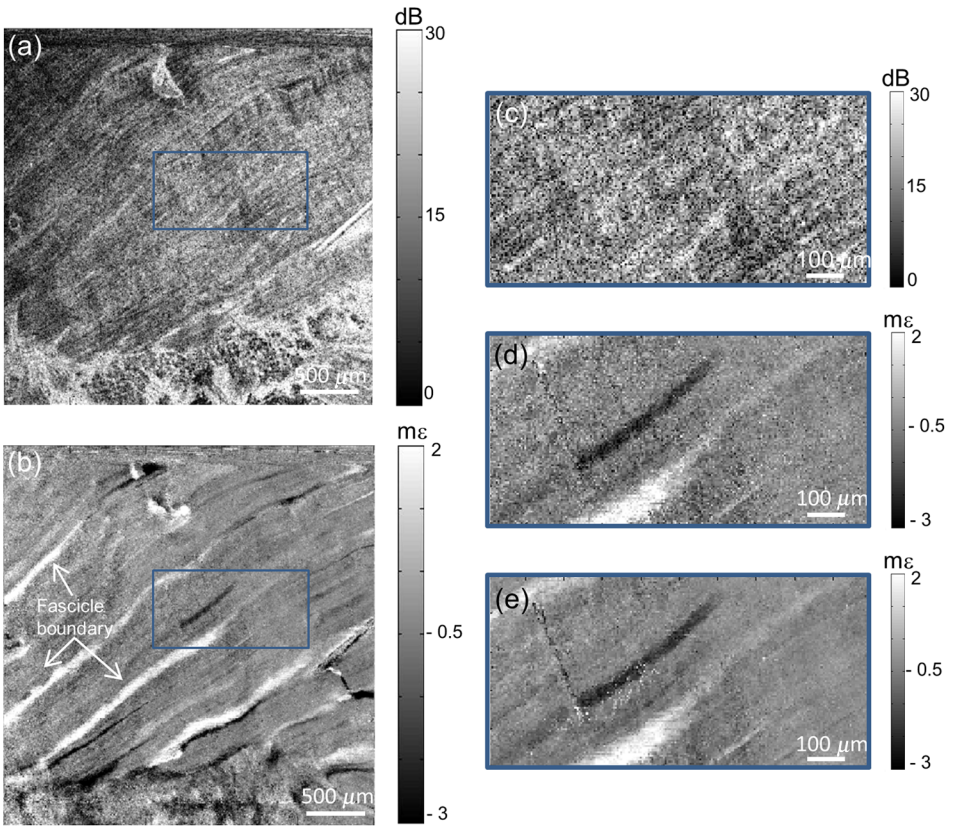

Fig. 4 *En face* (a) optical coherence tomography image and (b) elastogram (optical depth, 100 μm) of a 5-mm thick section of *ex vivo* gastrocnemius rat muscle. (c and d) Magnifications of the regions highlighted by a blue rectangle in (a) and (b). (e) Averaged magnified elastogram from five C-scan pairs.

displacement sensitivity. Wang et al. reported a strain sensitivity of 26 $\mu\varepsilon$ based on an OCT SNR of 50 dB (reported as a strain rate of 2.6×10^{-4} s^{-1} at 0.1 s acquisition time).[12] Although such SNRs can certainly be achieved at the surface of turbid tissue, dark speckles and attenuation limit the feasibility of achieving such high SNR at each pixel over the depth range (50 to 200 μm) required to calculate local strain. To improve the strain sensitivity in the presence of the lower OCT SNR in turbid tissue, our group has previously performed averaging of 50 loaded and unloaded B-scan pairs to achieve strain sensitivity of <3 $\mu\varepsilon$.[16,42]

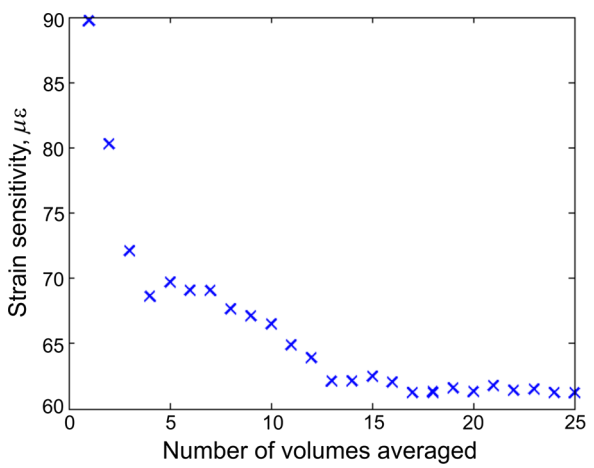

Fig. 5 Experimental characterization of strain sensitivity in the C-scan method versus number of 5-s scans averaged. Measurements taken with Phantom 1.

This level of averaging could be achieved in 3-D OCE using the technique described above (Fig. 5), but would result in a long acquisition time of >250 s.

The application of 3-D OCE to clinical and *in vivo* applications will require not only rapid acquisition of 3-D elastograms, as provided by our method, but also rapid processing to enable "live" visualization of the data acquired. This could be achieved by employing graphics processing units, as demonstrated for OCT[48] and Doppler OCT.[49]

5 Conclusion

We have demonstrated for the first time 3-D-OCE performed by calculating the phase difference between consecutive OCT C-scans, acquired before and after imparting a compressive load to a silicone phantom or freshly excised rat muscle. We demonstrated a 3-D-OCE acquisition time of 5 s, an order of magnitude shorter than with our existing B-scan method,[13,16] with displacement and strain sensitivity, 0.86 nm and 90 $\mu\varepsilon$, respectively, which are comparable to the B-scan method. We demonstrated that averaging improves the strain sensitivity to 60 $\mu\varepsilon$, at the expense of longer acquisition time. We expect that the increase in acquisition speed provided by this method will aid in the translation of OCE to clinical and *in vivo* applications.

Acknowledgments

We thank Gavin Pinniger and Jeremy Costin for providing access to muscle tissue and performing the dissection procedures. We also thank Kelsey Kennedy and Shaghayegh Es'haghian for useful discussions and the provision of

phantoms. L. Chin is supported by a Robert and Maude Gledden Postgraduate Research Scholarship from The University of Western Australia.

References

1. K. J. Parker et al., "A unified view of imaging the elastic properties of tissue," *J. Acoust. Soc. Am.* **117**(5), 2705–2712 (2005).
2. Y. C. Fung, *Biomechanics: Mechanical Properties of Living Tissues*, Springer-Verlag, New York (1981).
3. M. M. Doyley and K. J. Parker, "Elastography: general principles and clinical applications," *Ultrasound Clin.* **9**(1), 1–11 (2014).
4. J. Schmitt, "OCT elastography: imaging microscopic deformation and strain of tissue," *Opt. Express* **3**(6), 199–211 (1998).
5. B. F. Kennedy, K. M. Kennedy, and D. D. Sampson, "A review of optical coherence elastography: fundamentals, techniques and prospects," *IEEE J. Sel. Top. Quantum* **20**(2), 7101217 (2014).
6. R. Chan et al., "OCT-based arterial elastography: robust estimation exploiting tissue biomechanics," *Opt. Express* **12**(19), 4558–4572 (2004).
7. A. Chau et al., "Mechanical analysis of atherosclerotic plaques based on optical coherence tomography," *Ann. Biomed. Eng.* **32**(11), 1494–1503 (2004).
8. J. Rogowska et al., "Optical coherence tomographic elastography technique for measuring deformation and strain of atherosclerotic tissues," *Heart* **90**(5), 556–562 (2004).
9. H. J. Ko et al., "Optical coherence elastography of engineered and developing tissue," *Tissue Eng.* **12**(1), 63–73 (2006).
10. S. G. Adie et al., "Audio frequency in vivo optical coherence elastography," *Phys. Med. Biol.* **54**(10), 3129–3139 (2009).
11. S. J. Kirkpatrick et al., "Imaging the mechanical stiffness of skin lesions by in vivo acousto-optical elastography," *Opt. Express* **14**(21), 9770–9779 (2006).
12. R. K. Wang, S. Kirkpatrick, and M. Hinds, "Phase-sensitive optical coherence elastography for mapping tissue microstrains in real time," *Appl. Phys. Lett.* **90**(16), 164105 (2007).
13. B. F. Kennedy et al., "Strain estimation in phase-sensitive optical coherence elastography," *Biomed. Opt. Express* **3**(8), 1865–1879 (2012).
14. A. Nahas et al., "3D static elastography at the micrometer scale using full field OCT," *Biomed. Opt. Express* **4**(10), 2138–2149 (2013).
15. V. Y. Zaitsev et al., "A correlation-stability approach to elasticity mapping in optical coherence tomography," *Laser Phys. Lett.* **10**(6), 065601 (2013).
16. B. F. Kennedy et al., "Optical coherence micro-elastography: mechanical contrast imaging of tissue microstructure," *Biomed. Opt. Express* **5**(7), 2113–2124 (2014).
17. S. G. Adie et al., "Spectroscopic optical coherence elastography," *Opt. Express* **18**(25), 25519–25534 (2010).
18. C. Li et al., "Quantitative elastography provided by surface acoustic waves measured by phase-sensitive optical coherence tomography," *Opt. Lett.* **37**(4), 722–724 (2012).
19. K. D. Mohan and A. L. Oldenburg, "Elastography of soft materials and tissues by holographic imaging of surface acoustic waves," *Opt. Express* **20**(17), 18887–18897 (2012).
20. S. Wang et al., "Noncontact measurement of elasticity for the detection of soft-tissue tumors using phase-sensitive optical coherence tomography combined with a focused air-puff system," *Opt. Lett.* **37**(24), 5184–5186 (2012).
21. S. Wang et al., "A focused air-pulse system for optical-coherence-tomography-based measurements of tissue elasticity," *Laser Phys. Lett.* **10**(7), 075605 (2013).
22. V. Crecea et al., "Magnetomotive nanoparticle transducers for optical rheology of viscoelastic materials," *Opt. Express* **17**(25), 23114–23122 (2009).
23. V. Crecea, A. Ahmad, and S. A. Boppart, "Magnetomotive optical coherence elastography for microrheology of biological tissues," *J. Biomed. Opt.* **18**(12), 121504 (2013).
24. W. Qi et al., "Resonant acoustic radiation force optical coherence elastography," *Appl. Phys. Lett.* **103**(10), 103704 (2013).
25. W. Qi et al., "Phase-resolved acoustic radiation force optical coherence elastography," *J. Biomed. Opt.* **17**(11), 110505 (2012).
26. A. Nahas et al., "From supersonic shear wave imaging to full-field optical coherence shear wave elastography," *J. Biomed. Opt.* **18**(12), 121514 (2013).
27. M. Razani et al., "Feasibility of optical coherence elastography measurements of shear wave propagation in homogeneous tissue equivalent phantoms," *Biomed. Opt. Express* **3**(5), 972–980 (2012).
28. A. Srivastava et al., "Determination of elastic properties of resected human breast tissue samples using optical coherence tomographic elastography," *Strain* **47**(1), 75–87 (2011).
29. K. M. Kennedy et al., "Needle optical coherence elastography for the measurement of microscale mechanical contrast deep within human breast tissues," *J. Biomed. Opt.* **18**(12), 121510 (2013).
30. F. M. Hendriks et al., "The relative contributions of different skin layers to the mechanical behavior of human skin in vivo using suction experiments," *Med. Eng. Phys.* **28**(3), 259–266 (2006).
31. B. F. Kennedy et al., "In vivo dynamic optical coherence elastography using a ring actuator," *Opt. Express* **17**(24), 21762–21772 (2009).
32. X. Liang and S. A. Boppart, "Biomechanical properties of in vivo human skin from dynamic optical coherence elastography," *IEEE Trans. Biomed. Eng.* **57**(4), 953–959 (2010).
33. B. F. Kennedy et al., "In vivo three-dimensional optical coherence elastography," *Opt. Express* **19**(7), 6623–6634 (2011).
34. M. R. Ford et al., "Method for optical coherence elastography of the cornea," *J. Biomed. Opt.* **16**(1), 016005 (2011).
35. C. Li et al., "Noncontact all-optical measurement of corneal elasticity," *Opt. Lett.* **37**(10), 1625–1627 (2012).
36. A. S. Khalil et al., "Tissue elasticity estimation with optical coherence elastography: toward mechanical characterization of in vivo soft tissue," *Ann. Biomed. Eng.* **33**(11), 1631–1639 (2005).
37. G. van Soest et al., "Robust intravascular optical coherence elastography by line correlations," *Phys. Med. Biol.* **52**(9), 2445–2458 (2007).
38. M. Wojtkowski et al., "Three-dimensional retinal imaging with high-speed ultrahigh-resolution optical coherence tomography," *Ophthalmology* **112**(10), 1734–1746 (2005).
39. J. L. Whitwell et al., "3D maps from multiple MRI illustrate changing atrophy patterns as subjects progress from mild cognitive impairment to Alzheimer's disease," *Brain* **130**(7), 1777–1786 (2007).
40. O. Peters et al., "Three-dimensional analysis of root canal geometry by high-resolution computed tomography," *J. Dent. Res.* **79**(6), 1405–1409 (2000).
41. R. K. Wang, Z. Ma, and S. J. Kirkpatrick, "Tissue Doppler optical coherence elastography for real time strain rate and strain mapping of soft tissue," *Appl. Phys. Lett.* **89**(14), 144103 (2006).
42. K. M. Kennedy et al., "Analysis of mechanical contrast in optical coherence elastography," *J. Biomed. Opt.* **18**(12), 121508 (2013).
43. B. Park et al., "Real-time fiber-based multi-functional spectral-domain optical coherence tomography at 1.3 μm," *Opt. Express* **13**(11), 3931–3944 (2005).
44. A. Curatolo, B. F. Kennedy, and D. D. Sampson, "Structured three-dimensional optical phantom for optical coherence tomography," *Opt. Express* **19**(20), 19480–19485 (2011).
45. G. Lamouche et al., "Review of tissue simulating phantoms with controllable optical, mechanical and structural properties for use in optical coherence tomography," *Biomed. Opt. Express* **3**(6), 1381–1398 (2012).
46. J. W. Goodman, *Statistical Optics*, Wiley-Interscience, New York (1985).
47. W. Wieser et al., "Multi-megahertz OCT: high quality 3D imaging at 20 million A-scans and 4.5 GVoxels per second," *Opt. Express* **18**(14), 14685–14704 (2010).
48. Y. Watanabe and T. Itagaki, "Real-time display on Fourier domain optical coherence tomography system using a graphics processing unit," *J. Biomed. Opt.* **14**(6), 060506 (2009).
49. M. Sylwestrzak et al., "Four-dimensional structural and Doppler optical coherence tomography imaging on graphics processing units," *J. Biomed. Opt.* **17**(10), 100502 (2012).

Brendan F. Kennedy is research assistant professor in the Optical+ Biomedical Engineering Laboratory at The University of Western Australia. He received his PhD from Dublin City University, Ireland, in 2006. From 2006 to 2007, he was employed as lecturer in the Electrical Engineering Department, Universidad de Santiago de Chile. Since 2008, he has worked at The University of Western

Australia. His principle research interests are optical elastography and the measurement of tissue mechanics.

Francisco Gomes Malheiro received the BS degree in biomedical engineering and biophysics from the Faculty of Sciences, University of Lisbon, Portugal, in 2012. He is currently finishing his Master's degree in the same field, after completing a final year project during a 6-month internship in the Optical+Biomedical Engineering Laboratory, The University of Western Australia. His research interests include optical elastography and proton radiotherapy.

Lixin Chin is a PhD student in the Optical+Biomedical Engineering Laboratory within the School of Electrical, Electronic & Computer Engineering at The University of Western Australia. He is working in the areas of polarization-sensitive optical coherence tomography, compression optical coherence elastography, and their applications towards pre-clinical and clinical assessment of pathology.

David D. Sampson is director of the Centre for Microscopy, Characterisation & Analysis, a core facility of The University of Western Australia, and heads the Optical+Biomedical Engineering Laboratory (OBEL) in the School of Electrical, Electronic & Computer Engineering. He directs the Western Australian nodes of the Australian Microscopy & Microanalysis Research Facility and Australia's National Imaging Facility. He is a Fellow of the OSA and the SPIE and a senior member of the IEEE.